

See discussions, stats, and author profiles for this publication at: <https://www.researchgate.net/publication/261369781>

# A Fiber-Optic Sensor for Accurately Monitoring Biofilm Growth in a Hydrogen Production Photobioreactor

ARTICLE in ANALYTICAL CHEMISTRY · APRIL 2014

Impact Factor: 5.64 · DOI: 10.1021/ac500353y · Source: PubMed

---

CITATIONS

7

---

READS

80

## 4 AUTHORS, INCLUDING:



NB Zhong

Chongqing University of Technology

19 PUBLICATIONS 47 CITATIONS

[SEE PROFILE](#)



Xun Zhu

Sun Yat-Sen University

161 PUBLICATIONS 1,453 CITATIONS

[SEE PROFILE](#)

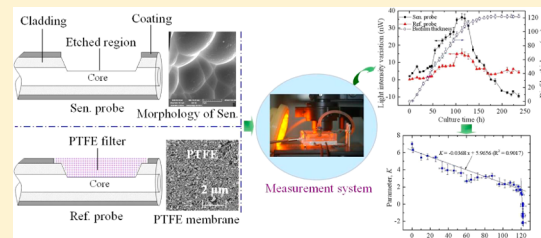
# A Fiber-Optic Sensor for Accurately Monitoring Biofilm Growth in a Hydrogen Production Photobioreactor

Nianbing Zhong<sup>†,‡</sup>, Qiang Liao,<sup>\*,†</sup> Xun Zhu,<sup>†</sup> and Rong Chen<sup>†</sup>

<sup>†</sup>Key Laboratory of Low-grade Energy Utilization Technologies and Systems, Chongqing University, Ministry of Education, Chongqing 400030, China

<sup>‡</sup>School of Optoelectronic Information, Chongqing University of Technology, Chongqing 400054, China

**ABSTRACT:** A new simple fiber-optic evanescent wave sensor was created to accurately monitor the growth and hydrogen production performance of biofilms. The proposed sensor consists of two probes (i.e., a sensor and reference probe), using the etched fibers with an appropriate surface roughness to improve its sensitivity. The sensor probe measures the biofilm growth and change of liquid-phase concentration inside the biofilm. The reference probe is coated with a hydrophilic polytetrafluoroethylene membrane to separate the liquids from photosynthetic bacteria *Rhodopseudomonas palustris* CQK 01 and to measure the liquid concentration. We also developed a model to demonstrate the accuracy of the measurement. The biofilm measurement was calibrated using an Olympus microscope. A linear relationship was obtained for the biofilm thickness range from 0 to 120  $\mu\text{m}$  with a synthetic medium under continuous supply to the bioreactor. The highest level of hydrogen production rate occurred at a thickness of 115  $\mu\text{m}$ .



A bacterial biofilm is an organized community of microorganisms attached to a support material under submersion or in contact with water.<sup>1</sup> The presence of biofilm in an industrial system can be detrimental or beneficial. For example, in the water industry, the optimized reuse of water in closed loop water circuits was contaminated by circuit fouling due to formation of biofilm, deposits, and scale formations.<sup>2</sup> Alternatively, effective bioremediation and biohydrogen require high-quality biofilm.<sup>3,4</sup> Especially, in the biohydrogen field, the biofilm attachment is considered a highly efficient technology for hydrogen production by photosynthetic bacteria (PSB).<sup>5</sup> The biofilm, therefore, has attracted intense interest for its potential advantages, including its high-conversion yield, avoidance of biomass-liquid separation, as well as its dual functions of wastewater biodegradation and hydrogen production. Although promising, the performance of biofilm photobioreactors (BPBRs) with PSB still experiences two critical problems: the biofilm thickness measurement and control.<sup>6</sup>

Monitoring biofilm growth is very important to control the biofilm thickness and enhance the BPBR's hydrogen production performance. As the biofilm grows on the support material, biofilm activity is not proportional to the immobilized biomass but instead increases in thickness until it reaches an optimal level, known as the "active thickness".<sup>7,8</sup> Above this threshold level, the thicker biofilms are more likely diffusion limited, which leads to a decrease in the  $\text{H}_2$  production rate, light conversion efficiency, and substrate degradation efficiency. Thus, the hydrogen production performance of BPBRs is still problematic for an uncontrolled biofilm. The optimization and control of the biofilm thickness depends on information obtained from monitoring the biofilm formation and growth.<sup>9</sup>

Thus, it is vital to develop a sensor to continuously and noninvasively monitor the growth of biofilms.

In the past 30 years, various techniques have been developed to monitor the biofilm progression, which can be divided into two different categories.<sup>10,11</sup> The first is offline testing, which requires partial or total biofilm removal from the BPBR. Among these techniques, the most frequently used are dry weight and microscopy imaging (epifluorescence, confocal laser-scanning, and atomic force microscopy).<sup>12,13</sup> Microscopy imaging can provide detailed information on the physical structure, cell size and shape, as well as chemical properties. However, the technique is slow, labor intensive, and intrusive, and therefore, incapable of providing real-time control at an industrial scale.

Ideally, biofilm information should be acquired online and be sensitive, accurate, fast, and nondestructive. The most common techniques for online and nondestructive measurements consist of optical methods (fiber-optic sensors,<sup>2</sup> spectroscopic ellipsometry,<sup>14</sup> photoacoustic spectroscopy,<sup>15</sup> and differential turbidity<sup>16</sup>); microelectrode methods based on changes in pH, oxygen, and hydrogen decreases due to biofilm accumulation;<sup>17</sup> electrochemical techniques (impedance and capacitance);<sup>18</sup> video microscopy;<sup>1</sup> and ultrasound.<sup>19</sup> Among these, fiber-optic sensors have attractive properties because of their microstructure, corrosion-resistance, immunity from electromagnetic interference, fast response speed, good biocompatibility, and easy installation. Thus, fiber sensors are suitable for application

Received: January 25, 2014

Accepted: March 25, 2014

Published: March 26, 2014



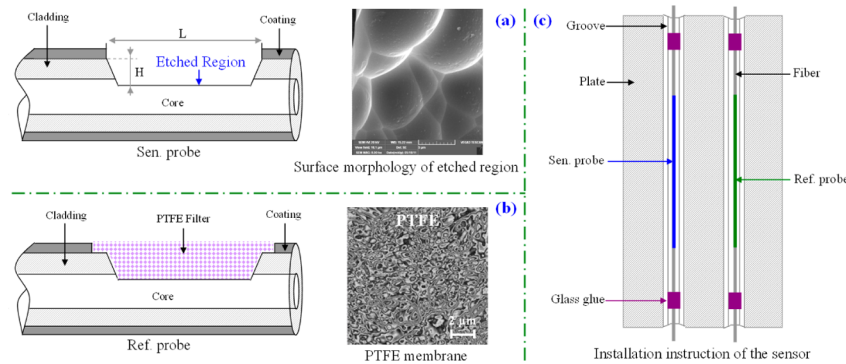


**Figure 1.** (a) Structural representation and SEM image of the Sen. probe. (b) Structural representation and microscope image of the ref. probe. (c) Installation instruction of the sensor.

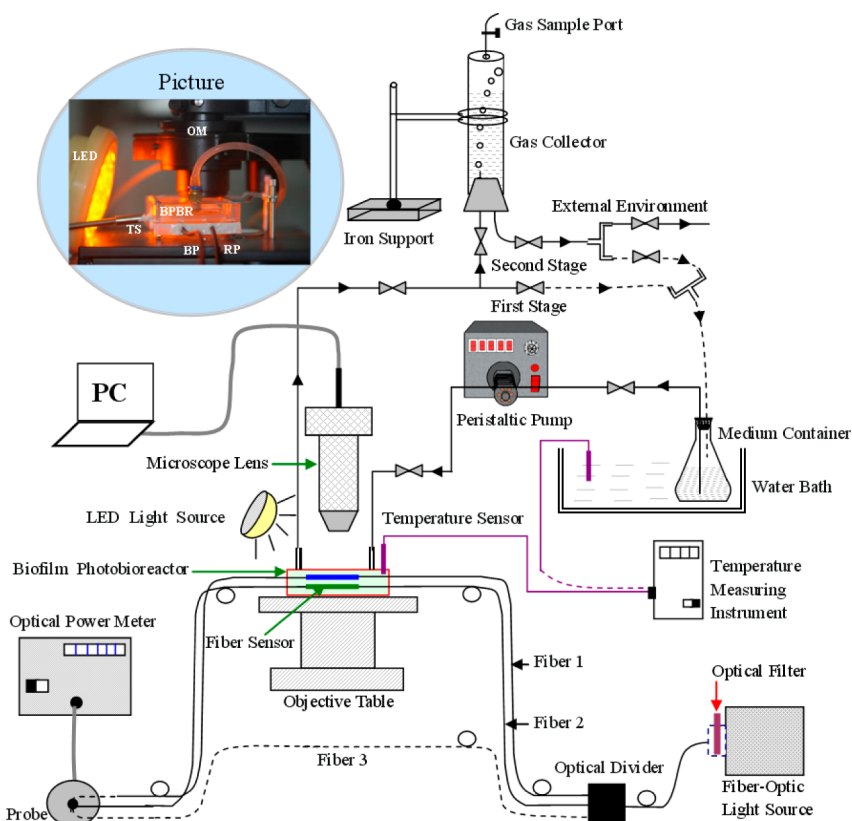


**Figure 2.** Schematic diagram of the experimental system (OM: optical microscope, TS: temperature sensor, BP: Sen. probe, and RP: ref. probe).

in the long term operation of BPBRs to precisely control biofilm growth.

Unfortunately, fiber sensors are difficult to use in practice. The biofilm is an extracellular material consisting of microbial cells, extracellular polymeric substances (EPS), and water.<sup>20</sup> The bacteria in the inner layer may decay and die when the biofilm is beyond its critical thickness because of substrate limitations.<sup>21</sup> Accordingly, the liquid-phase concentration and composition change with biofilm growth, owing to the increase in mass transfer resistance and change of metabolic pathways.<sup>22</sup> Thus, it is difficult for traditional fiber sensors to distinguish the effect of various factors (both biofilm biomass and liquid) on the biofilm thickness by only measuring the output signal. Additionally, the most commonly used fiber sensors are based on the evanescent-wave absorption,<sup>2</sup> of which the designers have not investigated the effect of thinned fiber surface

roughness on the light transmission properties or sensitivity, which leads to a lower overall sensitivity.<sup>23</sup> Hence, to accurately monitor biofilm growth in a bioreactor, it is important to create a high-sensitivity fiber-optic sensor that can separate the effects of biomass and liquid on the output signal.

In this work, we create a new fiber-optic evanescent wave (FOEW) sensor with two probes using etched fibers. A theoretical model of the proposed sensor is established. Its output signal is only a function of the bulk absorption coefficient and the refractive index of the biofilm. We also examined the sensor's optical transmission, temperature response, and the response speed of the reference probe. The biofilms were cultured with a continuous supply of a synthetic medium and monitored using the designed sensor. Furthermore, the biofilm measurements were calibrated with micro-

scope observations, and the hydrogen production rates of the biofilm were measured.

## MATERIALS AND METHODS

**Configuration of the Biofilm Sensor.** The two probes for the sensor were made from multimode silica optical fibers (Beijing Glass Research Institute R&D Center, China) with a core diameter of  $400 \pm 8 \mu\text{m}$ , cladding diameter of  $440 \pm 8 \mu\text{m}$ , coating diameter of  $480 \pm 10 \mu\text{m}$ , and numerical aperture (NA) of 0.5. Following the literature,<sup>24,25</sup> the cladding was removed from one-half of the wire over a length of 5 cm, using a fluorhydric acid/water mixture, and the exposed core of the fiber was used as the sensing region (i.e., L and H of 5 cm and  $100 \mu\text{m}$ , respectively). The appropriate surface roughness of the etched fibers, which are given by  $2\delta/\Delta$ , where  $\delta$  is the average pit depth and  $\Delta$  the average pit diameter is 0.32 (Figure 1a). The definitions of  $\delta$  and  $\Delta$  can be found in ref 23. As shown in Figure 1a, the exposed core of the fiber can sense the biofilm growth and changes in its liquid-phase concentration. Herein, this sensor is known as the sensor (Sen.) probe. To accurately measure the biofilm growth (i.e., to eliminate the effect of liquid-phase changes on the thickness measurement), a second exposed fiber core was coated with a hydrophilic polytetrafluoroethylene (PTFE) membrane (thickness and hole diameters of 20 and  $0.22 \mu\text{m}$ , respectively; Minglie Science and Technology, China) to separate the liquids from the bacteria. The coated PTFE membrane probe, herein known as the reference (Ref.) probe, is used to sense the liquid concentration (Figure 1b). The probes were fixed on the plate (support material of the BPBR) with grooves of  $500 \mu\text{m}$  (depth and width). The installation of the sensor is shown in Figure 1c.

**Microorganism and Cultivation.** The *Rhodopseudomonas palustris* CQK 01 strain was employed as the PSB for photoheterotrophic hydrogen production. The cells were cultivated anaerobically with argon gas at  $30^\circ\text{C}$  for 96 h under illumination from a 590 nm light-emitting diode (LED) at 4000 lx. The initial pH value of the medium before incubation was adjusted to 7.0 by using NaOH solution.

**Systems and Operations.** Figure 2 shows a schematic illustration of the BPBR biohydrogen production and measurement systems. The flat-panel BPBR was fabricated from poly(methyl methacrylate) (PMMA) with a working volume of  $125 \times 80 \times 5 \text{ mm}^3$ . The external LED light source (4000 lx; 590 nm) was mounted on one side of the BPBR. The glucose-based synthetic wastewater was prepared according to ref 3. The synthetic wastewater, with a temperature of  $30^\circ\text{C}$ , continuously passed through the BPBR via a peristaltic pump at a volumetric flow rate of 228 mL/h. Before the PSB was inoculated into the bioreactor with 10% inoculum, the photobioreactor body was sterilized with formalin and then thoroughly washed with deionized water. The composition of the biogas was analyzed using a gas chromatograph (GC). The  $\text{H}_2$  production performance of the photobioreactor was mainly assessed by the  $\text{H}_2$  production rate ( $R_a$ ), which is defined as

$$R_a (\text{mmol/L/h}) = \frac{\text{cumulative } \text{H}_2 \text{ production (mmol)}}{\text{H}_2 \text{ evolution time (h)} \times \text{bioreactor volume (L)}} \quad (1)$$

The online biofilm measurement system consisted of the fibers, the Sen. and Ref. probes, an optical filter, a light source, and an optical power meter. Fibers 1 and 2 are connected to

the Sen. and Ref. probes, respectively. Fiber 3 is directly connected to the optical power meter (UV 0.2, Newport Corporation; obtained from NBeT Group Corp.) to identify changes in environmental light intensity. A broad-bandpass filter is used to only admit light between 410 and 1100 nm (LPF-400-01, DaHeng Optical Thin Film). The light source (DH-2000, Ocean Optics) consisted of deuterium tungsten halogen sources (deuterium lamp, 25 W and tungsten halogen lamp, 20 W), operating in the 190–2000 nm range. The power meter had a wavelength range of 200–1100 nm, power range of 100 pW to 0.2 W, and maximum uncertainty of 4%. To detect the temperature in the BPBR, a thermocouple with a  $500 \mu\text{m}$  diameter was employed. The optical microscope system (IX81, Olympus, Japan) with a resolution of  $\pm 1 \mu\text{m}$  was used to calibrate the biofilm thickness. For more details on the biofilm thickness test, see Ref 26.

**Principle of Measurement.** As shown in Figure 2, the effects of the changes to the liquid-phase concentration and environmental light intensity were examined using the detecting pathways of fibers 2 and 3, respectively. To establish the working principle of the sensor, we develop a theoretical model with the following steps. First, for the Sen. probe, according to our previous study on the effect of surface roughness on the light transmission properties and sensitivity of FOEW sensors,<sup>24</sup> the effective transmitted light intensity through a rough fiber, in which the evanescent waves have decayed, can be written as

$$I_{\text{out},1} = I_{\text{in},1} e^{-\xi_1 L} + \sigma_1 I_{\text{in},2} \quad (2)$$

where,  $I_{\text{in},1}$  is the effective incident light intensity from the fiber-optic light source,  $I_{\text{in},2}$  is the environmental light intensity,  $\xi_1$  is the decay coefficient of evanescent waves in the biofilm with a liquid mixture,  $\sigma_1$  is the effective optical coupling coefficient between the etched fiber region, and  $L$  is the length of the unclad (sensing) fiber region. The quantities  $I_{\text{in},1}$ ,  $\xi_1$ , and  $\sigma_1$  can be further expressed as

$$I_{\text{in},1} = \frac{\pi/2 - U_i - \frac{\delta_1}{2r} \arctan(2\delta_1/\Delta_1)}{\pi/2 - U_i} I_{\text{in}} = K_1 I_{\text{in}} \quad (3.1)$$

$$\begin{aligned} \xi_1 &= \frac{\lambda(\alpha_1 n_1 + \alpha_2 n_2)}{2\pi r n_r^2 \cos^3 \theta_c} \\ &= \frac{\cos^2 \left[ \frac{\pi}{2} - \arcsin \left( \frac{n_0}{n_r} \sin U_i \right) - \arctan(2\delta_1/\Delta_1) \right]}{\sin \left[ \frac{\pi}{2} - \arcsin \left( \frac{n_0}{n_r} \sin U_i \right) - \arctan(2\delta_1/\Delta_1) \right]} \\ &= \frac{\lambda(\alpha_1 n_1 + \alpha_2 n_2)}{2\pi r n_r^2 \cos^3 \theta_c} \cdot K_2 \end{aligned} \quad (3.2)$$

$$\sigma_1 = f(\delta_1, \Delta_1) \quad (3.3)$$

where  $U_i$  is the angle of light rays on the input end of the fiber, ranging from 0 to  $U_{\max}$ ;  $\delta$  and  $\Delta$  are the average pit depth and average pit diameter, respectively, for the rough fiber surface (Figure 1a);  $I_{\text{in}}$  is the incident light intensity at the input end of the fiber,  $\alpha_1$  and  $n_1$  are the bulk decay coefficient and refractive index of the microbial cells in the biofilm, respectively;  $\alpha_2$  and  $n_2$  are the bulk decay coefficient and refractive index of the liquid mixture in the biofilm, respectively;  $r$  is the fiber radius in the thinned region;  $n_r$  is the refractive index of the etched-fiber core at a radius  $r$ ;  $\theta_c$  is the critical angle for total reflection at

the core-cladding interface of a typical fiber;  $n_0$  is the refractive index of air; and  $\sigma_1$  is a function of  $\delta_1$  and  $\Delta_1$ .  $U_{\max}$  is the maximum incidence angle of the light rays on the input end of the fiber, and is given by  $U_{\max} = \arcsin[(\text{NA})/(n_0)] = \arcsin[(1)/(n_0)(n_{\max}^2 - n_R^2)^{1/2}]$ , where NA is the numerical aperture of a typical optical fiber and  $n_R$  is the refractive index of the fiber core at radius  $R$ .

For the Ref. probe, the effective transmitted light intensity through fiber 2 (Figure 2), in which the evanescent waves have decayed, can be written as,

$$I_{\text{out},2} = I_{\text{in},3} e^{-\xi_2 L} + \sigma_2 I_{\text{in},2} \quad (4)$$

where  $I_{\text{in},3}$  is the effective incident light intensity from the fiber-optic light source,  $\xi_2$  is the decay coefficient of evanescent waves in the liquid mixture, and  $\sigma_2$  is the effective optical coupling coefficient between the etched fiber region and environmental light intensity. The quantities  $I_{\text{in},3}$ ,  $\xi_3$ , and  $\sigma_2$  can be expressed as

$$I_{\text{in},3} = \frac{\pi/2 - U_i - \frac{\delta_2}{2r} \arctan(2\delta_2/\Delta_2)}{\pi/2 - U_i} I_{\text{in}} = K_3 I_{\text{in}} \quad (5.1)$$

$$\begin{aligned} \xi_2 &= \frac{\lambda \alpha_2 n_2}{2\pi r n_r^2 \cos^3 \theta_c} \cdot \\ &\frac{\cos^2 \left[ \frac{\pi}{2} - \arcsin \left( \frac{n_0}{n_r} \sin U_i \right) - \arctan(2\delta_2/\Delta_2) \right]}{\sin \left[ \frac{\pi}{2} - \arcsin \left( \frac{n_0}{n_r} \sin U_i \right) - \arctan(2\delta_2/\Delta_2) \right]} \\ &= \frac{\lambda \alpha_2 n_2}{2\pi r n_r^2 \cos^3 \theta_c} \cdot K_4 \end{aligned} \quad (5.2)$$

$$\sigma_2 = f(\delta_2, \Delta_2) \quad (5.3)$$

In this work, the ambient light is mainly from the LED and sunlight that is coming through the window. In accordance with the detecting pathways of Fiber 3 (Figure 2), the light intensity was about 4 nW when the fiber-optic light source was turned off. However, the initial light intensity from the fiber-optic light source in the fiber was above 250 nW for Fibers 1 to 3 (Figure 2). Hence, the effect of environmental light on the probes can be ignored, and eqs 2 and 4 can be simplified to

$$\begin{cases} I_{\text{out},1} = K_1 I_{\text{in}} e^{-\xi_1 L} \\ I_{\text{out},2} = K_3 I_{\text{in}} e^{-\xi_2 L} \end{cases} \quad (6)$$

In accordance with eqs 3.2 and 5.2, when the ratio  $2\delta_1/\Delta_1$  is approximately equal to  $2\delta_2/\Delta_2$ ,  $K_2$  is approximately equal to  $K_4$ . Thus, by using eqs 3.2, 5.2, and 6, the output signal of the sensor can be expressed as,

$$K = \frac{I_{\text{out},1}}{I_{\text{out},2}} = \frac{K_1}{K_3} \exp \left( -\frac{\lambda \alpha_1 n_1}{2\pi r n_r^2 \cos^3 \theta_c} \cdot K_2 \right) \quad (7)$$

As eq 7 shows, the output signal  $K$  is a function of  $\alpha_1$  and  $n_1$ , when  $r$ ,  $n_r$ ,  $\delta_p$ , and  $\Delta_j$  ( $j = 1, 2$ ) are constant, and  $K$  is not affected by changes in the liquid phase composition or concentration. Philip-Chandy et al.<sup>2</sup> discovered that the refractive index of biofilms from mixed bacteria is over the range from 1.330 to 1.355 when the biofilm thickness ranges from 0 to 2 mm. There will be a one-to-one correspondence

between the biofilm thickness and its refractive index. Thus, we can determine the biofilm thickness by using the parameter  $K$ .

## EXPERIMENTAL RESULTS AND DISCUSSION

**Sensor Performance Parameters.** The sensitivity and accuracy of the sensor depends on the attenuation of the evanescent waves, which is affected by the effective transmission light intensity, temperature sensitivity, and time response of the probes. Hence, before we monitor the biofilm growth, we must first examine the sensor performance parameters, including the optical transmission and temperature response. The response time of the Ref. probe and the sensitivity of the Sen. probe was examined using a glucose solution.

**Spectral Transmission of the Probes.** To perform the optical transmission test, the etched fibers were kept straight and placed in a light tight box filled with air at 30 °C. The transmitted light intensity was measured using an optical spectrometer (QE65000, Oceanoptics) with a spectral resolution of 0.14–7.7 nm between 200 and 1150 nm. The total spectral scanning time was 1 s for all tests. Figure 3 shows the spectral transmission of the etched fibers.

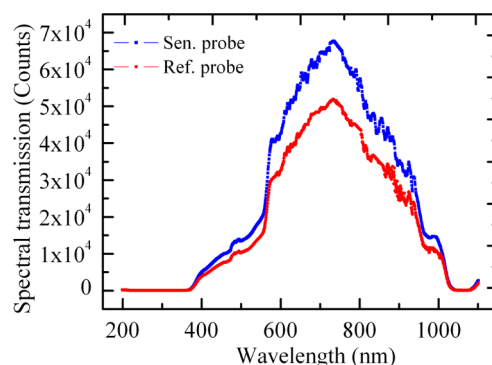


Figure 3. Spectral transmission characteristics of the Sen. and Ref. probes.

The spectral transmission power of the etched fibers is different in the two probes. This is because the scattering and refraction at the unclad surface causes ineffective optical transmissions,<sup>23</sup> and the evanescent waves decay from the rough surfaces of the fibers.<sup>27</sup> Both effects cause a loss in transmitted intensity. Furthermore, although the fibers were prepared in the same etching conditions, the local pit depth can vary because of different etching rates caused by local compositional differences in the fiber core.<sup>25</sup> The surface pit size can significantly impact the transmitted light power,<sup>23</sup> which causes the spectral transmission properties of etched fibers to vary.

**Temperature Response of Probes.** To investigate the effect of the temperature on the light transmission intensity of the etched fibers, the fibers were kept straight and immersed into a thermostatic water bath. The test temperature was varied between 25 and 40 °C to suit most of the PSB strains. We discovered that the output light intensity variation (i.e.,  $\Delta I_T = I_T - I_1$ ), where  $I_T$  is the output light intensity at temperature  $T$  and  $I_1$  is the initial output light intensity at 25 °C, only increases slightly with an increase in temperature because of the thermal deformation of the fiber and change in the refractive index of water. However, the maximum  $\Delta I_T$  is still less than 0.03 nW. The light transmission intensity of the etched fibers is

about 250 nW at 25 °C, thus the effect of temperature on the output light intensity of the probes can be ignored between 25 to 40 °C. In other words, the performance of the proposed sensor is independent of temperature.

**Response Time of the Ref. Probe.** The response time of the Ref. probe may be affected by the physical–chemical properties of the membrane filter applied. To investigate the performance, we repeatedly examined the response time to changes in glucose concentration. The experiment was performed at 30 °C, as follows. First, the Ref. probe was immersed into distilled water for approximately 2 min to thoroughly soak the PTFE membrane. Afterward, the soaked probe was removed and inserted into a test container with a glucose solution of 3 g/100 mL. Once the output light intensity was stable, the probe was immediately inserted into distilled water. This second step was repeated several times. Figure 4 shows three typical probe responses at a sampling interval of 5 s.

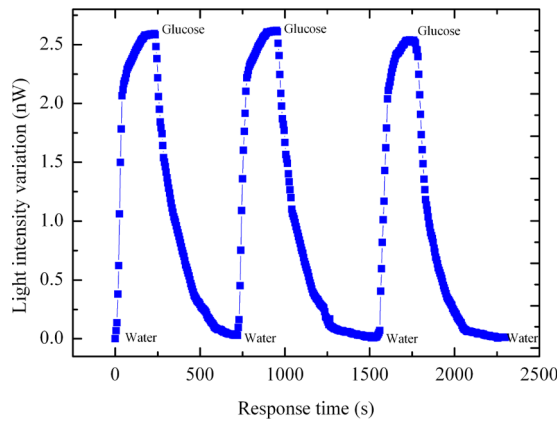


Figure 4. The time response curve of the Ref. probe.

One can see that  $\Delta I_\tau$  varies (i.e.  $\Delta I_\tau = I_\tau - I_2$ , where  $I_\tau$  is the output light intensity at time  $\tau$  and  $I_2$  is the initial output light intensity of the Ref. probe through the distilled water at 30 °C) significantly as a function of glucose concentration. The  $\Delta I$  rapidly increased with increasing time when the probe was inserted into the glucose solution and slowly reached a relatively stable value, as the immersion time increased. The reverse behavior was similar. The response times of the  $\Delta I_\tau$  increase and decrease were 240 and 400 s, respectively. This can be attributed to the fact that the surrounding concentration of the etched fiber region is controlled by the diffusion rate of the glucose through the PTFE membrane.<sup>28</sup> The maximum  $\Delta I_\tau$  was 2.58 nW consistently. This shows that the Ref. probe can respond quickly to the changes in the liquid-phase concentration.

**Sensitivity of the Probes.** To investigate the sensitivity of the probes, we first installed the probes on the floor of the BPBR, as shown in Figure 1c and then prepared glucose-based test solutions as an absorbing medium by mixing glucose ( $C_6H_{12}O_6 \cdot H_2O$ , 99%) and distilled water. The concentrations of the solutions varied between 0 and 30 g/100 mL, and the refractive index varied between 1.3319 and 1.3669 at 30 °C (the refractive index was measured by a refractometer, NAR-1T solid, ATAGO, Japan). The glucose solutions were pumped into the BPBR with a peristaltic pump at a volumetric flow rate of 48 mL/h. Each concentration remained for 10 min before it was driven out of the BPBR for the next use. Figure 5 shows the

light intensity variation as a function of the glucose concentration at 30 °C.

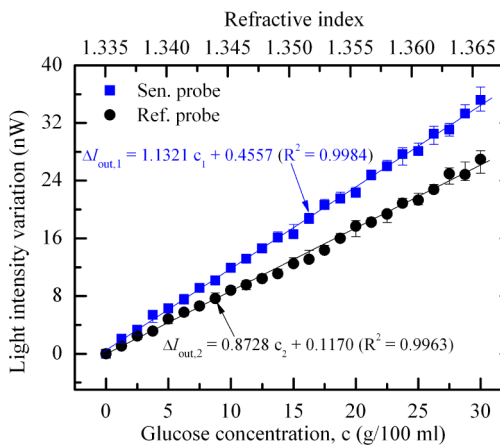


Figure 5. Output light intensity variation of the probes as a function of glucose concentration.

One can see that  $\Delta I_c$  (i.e.  $\Delta I_c = I_c - I_3$ , where  $I_c$  is the output light intensity at glucose concentration  $c$  and  $I_3$  is the initial output light intensity of the probes through the distilled water at 30 °C) increased with increasing glucose concentration. This can be explained as follows. First, the refractive index of the solution increases with an increasing glucose concentration, thereby indicating that the difference in the refractive index between the silica and glucose solution decreases.<sup>29</sup> This means that the random scattering and refraction of light at the pits on the fiber surface decreases. Second, in the glucose solution, no light absorption occurs in the 410–1100 nm spectral region. Hence, the transmitted intensity of the light would not be affected by the evanescent field intensity, according to the evanescent wave theory. The variation of light intensity of the Sen. probe is larger than that of the Ref. probe because the former has a better effective light transmission capacity, as shown in Figure 3.

**Biofilm Measurement.** Liao et al.<sup>13</sup> discovered that the biofilm formation and structure is significantly affected by the culture conditions, such as the illumination wavelengths and intensities, pH, temperature, flow rates, and substrate concentration for the particular bacterial strain. Stoodley et al.<sup>30</sup> and Goeres et al.<sup>31</sup> also reported that the biofilm growth rate and structure developed differently between steady-state and continuous-flow cultures, owing to the effects of fluid shear and substrate as well as product inhibition. Hence, for a biofilm attached to the fiber-sensing region, the sensor response will be affected by the biofilm culture conditions.

Currently, biofilm biohydrogen production using a continuous flow culture is one of the most commonly used methods to obtain a continuous production of hydrogen.<sup>13,32</sup> To simplify and accurately assess the performance of the sensor, the biofilm growth was investigated for continuous flow cultures. In this work, the continuous flow biofilm culture was performed after two preparatory steps. First, the bacterial suspension (optical density  $OD_{600\text{ nm}}$  and pH of 0.45 and 7.0, respectively) was prepared using cultivated bacteria and sterilized distilled water. The bacteria suspension was recycled with a flow rate of 48 mL/h for approximately 4 h to avoid the loss of activated PSB cells in the circulated liquid solution. Second, the bacteria suspension-filled BPBR was maintained at

a steady-state for 20 h to avoid desorption of the cells. Thereafter, continuous operation can be performed. At this stage, the fresh nutrient medium flow rate was 48 mL/h, and the operation temperature was maintained at 30 °C to obtain a high biofilm growth rate and hydrogen production rate. Figure 6 shows the probe responses to the biofilm growth process. To

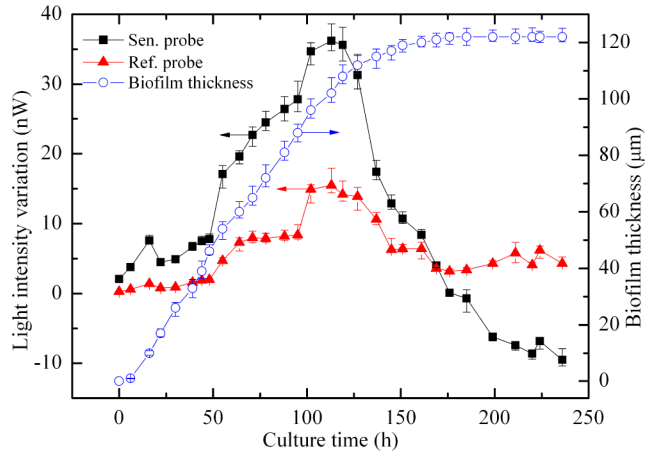


**Figure 6.** Output signal of the sensor probes and biofilm thickness as a function of culture time.

calibrate the sensor, the biofilm development was also monitored with an Olympus microscope. The results of which are shown in Figure 6.

Figure 6 shows that the  $\Delta I$  (i.e.  $\Delta I = I_h - I_4$ , where  $I_h$  is the output light intensity at biofilm culture time  $h$  and  $I_4$  is the initial output light intensity of the probes through the PSB bacterial suspension at 30 °C) of the probes first increased then decreased during the initial biofilm formation stage. The refractive index difference between the fiber and surrounding medium decreased when the bacteria suspension was pumped into the BPBR; thus, the light transmission capacity of the fibers became enhanced and  $\Delta I$  increased. The  $\Delta I$  of both the Sen. and Ref. probes decreased because of the decrease in the

substrate concentration; however, the Sen. probe  $\Delta I$  also decreased, owing to the decrease in evanescent wave intensity caused by the absorption of the biofilm cells.

Thereafter, the  $\Delta I$  for the continuous operation phase of the Sen. probe again increased and reached its highest level in approximately 113 h before decreasing again. This can be attributed to the fact that the metabolite concentration increased with an increase in the activity or number of PSB cells,<sup>33</sup> thus causing the mixed solution (substrate and product) concentration to increase. However, the cell density increased, and the porosity of the biofilm decreased with increasing culture time, as shown in Figure 7, thereby indicating that the mass transfer resistance increased.<sup>34</sup> Then, the substrate concentration at the fiber surface decreased. Furthermore, the evanescent wave attenuation was accelerated because it was absorbed by the denser cells when the biofilm thickness was greater than 102  $\mu\text{m}$  at a culture time of 108 h (Figure 7). As discussed above,  $\Delta I$  decreased when the culture time was greater than 108 h and biofilm thickness was greater than 102  $\mu\text{m}$ .

For the Ref. probe,  $\Delta I$  increased, then decreased, and finally approached a constant value. The  $\Delta I$  increase can also be interpreted as a substrate and product concentration increase. The  $\Delta I$  decrease can be explained as follows. When the biofilm attached to the PTFE membrane, the cell density and biofilm thickness increased with culture time, as shown in Figure 7, which led to an increase in the mass transfer resistance. Thus, the separated liquid phase concentration at the fiber surface and  $\Delta I$  both decreased. After that,  $\Delta I$  was maintained at a constant level. This can be attributed to the fact that the substrate and product from the biofilm diffused into the fiber surface (i.e., sensing region) and obtained equilibrium when the biofilm developed into a denser structure (as shown in Figure 7, sample D).

One can also clearly see that the biofilm growth experienced three phases: an adsorption phase, an exponential phase, and a stationary phase. In the adsorption phase, the biofilm structure was quite loose, as seen in Figure 7, sample A. When the biofilm entered the exponential phase, it changed into a denser

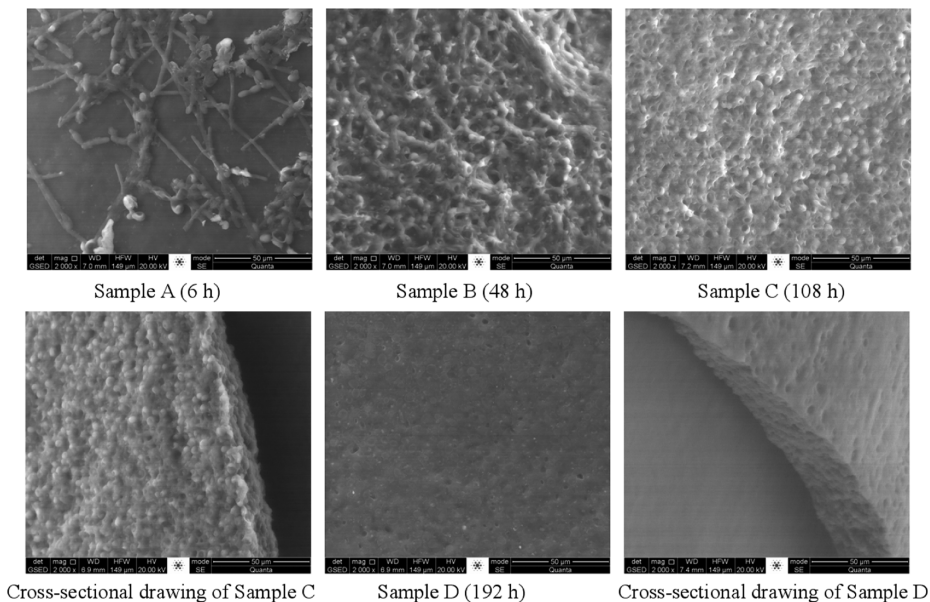


**Figure 7.** Environmental scanning electron microscope images of the biofilm at different culture times.

structure, as seen in Figure 7, samples B and C. Thereafter, with the biofilm uncontrolled, the porosity of the biofilm further decreased and its thickness maintained a constant level of 122  $\mu\text{m}$  because of product inhibition and substrate as well as light limitations, as seen in Figure 7, sample D. Furthermore, according to the error bars shown in Figure 6, we find that the maximum relative error of the Sen. probe, Ref. probe, and biofilm thickness were 11.2%, 16.5%, and 9.4%, respectively.

To obtain a quantitative relationship between the sensor output signal and biofilm thickness, the signals of the Sen. and Ref. probes were processed using eq 7. Figure 8 shows the value of  $K$  with different biofilm thicknesses ( $x$ ).

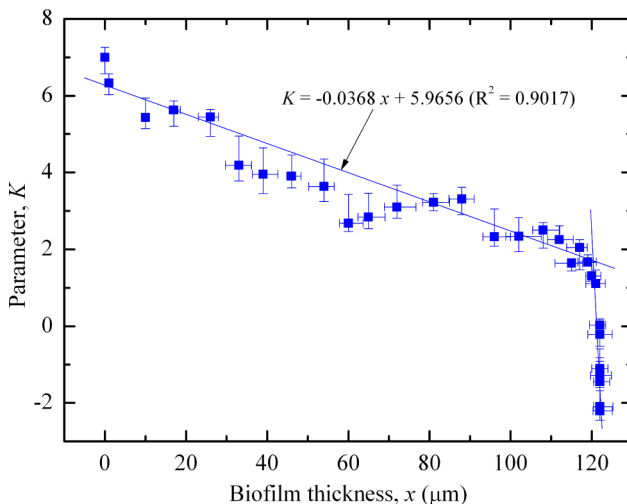


Figure 8. Parameter  $K$  as a function of the biofilm thickness  $x$ .

The parameter  $K$  decreases linearly with biofilm thickness  $x$  up to 120  $\mu\text{m}$ . The function can be expressed as  $K = -0.0368x + 5.9656$  ( $R^2 = 0.9017$ ). However, when the thickness is greater than 120  $\mu\text{m}$ ,  $K$  decreases much more rapidly. This can be explained as follows. The refractive index and density of the biofilm increases with biofilm thickness (i.e.,  $\alpha_1$  and  $n_1$  increases). According to eq 7,  $K$  decreases. The main reason that  $K$  decreases rapidly when the biofilm thickness is greater than 120  $\mu\text{m}$  is that the bottom biofilm cells gradually die and attach tightly to the surface of the fiber owing to the substrate and light limitations, which leads to the refractive index increasing significantly. Thus, when the biofilm was thicker than 120  $\mu\text{m}$ ,  $K$  responded poorly to further increases in the thickness. Effectively, the available measurement range of the sensor is between 0 and 120  $\mu\text{m}$ . Furthermore, we find that the maximum relative error between the fitted curve  $K$  and the calculated data from the experiment results (Figure 6) was 14.7% when the biofilm thickness was below 120  $\mu\text{m}$ .

**Biofilm Hydrogen Production Performance.** Biofilm thickness is a key factor that affects the biohydrogen production.<sup>35</sup> Thin biofilms with low cell concentrations exhibit a low  $\text{H}_2$  production rate and hydrogen yield. Meanwhile, when the biofilm thickness is greater than the active thickness, the biofilms are more likely to be diffusion limited. LaMotta<sup>7</sup> also confirmed that once a certain biofilm thickness is exceeded, substrate removal is not increased by a further accumulation of microorganisms on the support material. The biohydrogen production performance of BPBRs is also affected by the biofilm thickness and its structure.<sup>36</sup> In order to obtain a high biohydrogen production performance,

the effect of biofilm thickness on the hydrogen production rate was investigated. The biofilm was cultured under a continuous fresh nutrient medium. The biofilm growth process was monitored using the proposed sensors, and the conditions are identical to those described in Biofilm Measurement. Figure 9 shows the hydrogen production rate during the biofilm growth process.

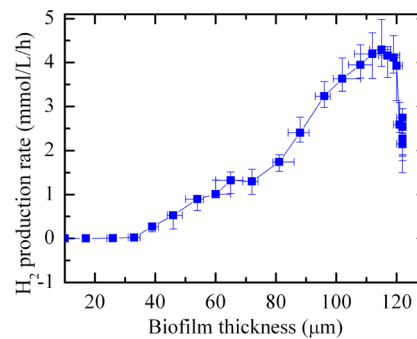


Figure 9.  $\text{H}_2$  production rate as a function of biofilm thickness.

Figure 9 shows that very little hydrogen was produced when the biofilm thickness was less than 60  $\mu\text{m}$ , which is during the exponential growth phase when the cells are dividing and reproducing. Thereafter, the  $\text{H}_2$  production rate increased slowly for biofilm thicknesses between 60 and 90  $\mu\text{m}$  because the biofilm matured more gradually and the biofilm cells were geared more toward the metabolic pathway of hydrogen production. At a thickness of about 115  $\mu\text{m}$ , the  $\text{H}_2$  production rate increased rapidly and reached a maximum of 4.2 mmol/L/h. However, the  $\text{H}_2$  production rate decreased rapidly for biofilm thicknesses greater than 115  $\mu\text{m}$ . For example, the rate reduced to 2.1 mmol/L/h at a thickness of approximately 120  $\mu\text{m}$ . To maintain a normal biofilm structure and avoid the detachment of the adhered cells as the thickness increases, the biofilm cells must produce large amounts of extracellular polymeric substances. As the EPS and number of cells increase, the porosity of the biofilm decreases, as shown in Figure 7. Thus, the mass transfer resistance and light decay increased, which leads to the bottom of the biofilm to suffer from substrate and light limitations as well as a product inhibition. This caused the biofilm hydrogen production capacity to decrease. One can see that the active thickness of the PSB CQK 01 biofilm is approximately 115  $\mu\text{m}$ . This information can guide researchers to improve the performance of biofilms for hydrogen production and wastewater treatment by controlling the biofilm thickness.

## CONCLUSIONS

A new and cost-effective biofilm thickness FOEW sensor was created from etched fibers with  $2\delta/\Delta = 0.32$ , and its theoretical model was established. The proposed sensor was applied to the study of biofilm growth with a continuous supply of fresh nutrient medium. Furthermore, the hydrogen production rate of a BPBR was investigated under various PSB CQK 01 biofilm thicknesses using the proposed sensor. The linear relationships between the sensor output signal and biofilm thickness in the range of 0 to 120  $\mu\text{m}$  were obtained:  $K = -0.0368x + 5.9656$  ( $R^2 = 0.9017$ ) for the continuous supply of the synthetic medium. Thus, the created sensor is effective at accurately monitoring the biofilm development online in a thickness range

between 0 and 120  $\mu\text{m}$ . In addition, we found that the active biofilm thickness was 115  $\mu\text{m}$ , which exhibited the highest hydrogen production rate of 4.2 mmol/L/h. This illustrates that these accurate, online, and nondestructive biofilm measurement technologies have great potential for applications in bioreactors by improving the performance of biofilms through controlling the formation process.

## AUTHOR INFORMATION

### Corresponding Author

\*E-mail: lqzx@cqu.edu.cn. Tel: +86-023-65102474. Fax: +86-023-65102474.

### Notes

The authors declare no competing financial interest.

## ACKNOWLEDGMENTS

This work was supported by the Key Projects of the National Natural Science Foundation of China (Grant 51136007) and the Key Projects of the Chongqing Municipal Natural Science Foundation of China (Grant cstc2013jjB9004).

## REFERENCES

- (1) Blanco, A.; Torres, E.; Fuente, E.; Negro, C. *Ind. Eng. Chem. Res.* **2011**, *50*, 5766–5773.
- (2) Philip-Chandy, R.; Scully, P. J.; Eldridge, P.; Kadim, H. J.; Gérard Grapin, M.; Guy Jonca, M.; Gérard D'Ambrosio, M.; Colin, F. [J]. *IEEE J. Sel. Top. Quantum Electron.* **2000**, *6*, 764–772.
- (3) Liao, Q.; Zhong, N. B.; Zhu, X.; Chen, R.; Wang, Y. Z.; Lee, D. J. *Int. J. Hydrogen Energy* **2013**, *38*, 15730–15737.
- (4) Singh, R.; Paul, D.; Jain, R. K. *Trends. Microbiol.* **2006**, *14*, 389–397.
- (5) Léonard, A.; Dandoy, P.; Danloy, E.; Leroux, G.; Meunier, C. F.; Rooke, J. C.; Su, B. L. *Chem. Soc. Rev.* **2011**, *40*, 860–885.
- (6) Androga, D. D.; Ozgur, E.; Gunduz, U.; Yucel, M.; Eroglu, I. *Int. J. Hydrogen Energy* **2011**, *36*, 11369–11378.
- (7) LaMotta, E. J. *Environ. Sci. Technol.* **1976**, *10*, 765–769.
- (8) Cheng, K. C.; Demirci, A.; Catchmark, J. M. *Appl. Microbiol. Biotechnol.* **2010**, *87*, 445–456.
- (9) Ludensky, M. *Int. Biodeterior. Biodegrad.* **2003**, *51*, 255–263.
- (10) Kristensen, G. H.; Christensen, F. R. *Water Res.* **1982**, *16*, 1619–1621.
- (11) Maurício, R.; Dias, C. J.; Jubilado, N.; Santana, F. *Environ. Monit. Assess.* **2013**, *10*, 8125–8133.
- (12) Yonezawa, H.; Osaki, T.; Kurata, S.; Fukuda, M.; Kawakami, H.; Ochiai, K.; Hanawa, T.; Kamiya1, S. *BMC Microbiol.* **2009**, *9*, 197.
- (13) Liao, Q.; Wang, Y. J.; Wang, Y. Z.; Zhu, X.; Tian, X.; Li, J. *Bioresour. Technol.* **2010**, *14*, 5315–5324.
- (14) Wang, B.; Wang, J.; Li, D.; Ren, K.; Ji, J. *Appl. Surf. Sci.* **2012**, *258*, 7801–7808.
- (15) Dole, M. N.; Patel, P. A.; Sawant, S. D.; Shedpure, P. S. *Int. J. Pharm. Sci. Rev. Res.* **2011**, *7*, 159–166.
- (16) Schmid, T.; Panne, U.; Adams, J.; Niessner, R. *Water Res.* **2004**, *38*, 1189–1196.
- (17) Costerton, J. W.; Lewandowski, Z.; Caldwell, D. E.; Korber, D. R.; Lappin-Scott, H. M. *Annu. Rev. Microbiol.* **1995**, *49*, 711–745.
- (18) Herbert-Guilhou, D.; Tribollet, B.; Festy, D.; Kiéné, L. *Electrochim. Acta* **1999**, *45*, 1067–1075.
- (19) Bott, T. R. *Heat Transfer Eng.* **2000**, *21*, 43–49.
- (20) Chandra, J.; Kuhn, D. M.; Mukherjee, P. K.; Hoyer, L. L.; McCormick, T.; Ghannoum, M. A. *J. Bacteriol.* **2001**, *183*, 5385–5394.
- (21) Liu, B.; Gu, L.; Yu, X.; Yu, G.; Zhang, H.; Xu, J. *Sci. Total Environ.* **2012**, *414*, 508–514.
- (22) Stewart, P. S. *J. Bacteriol.* **2003**, *185*, 1485–1491.
- (23) Zhong, N. B.; Zhu, X.; Liao, Q.; Wang, Y. Z.; Chen, R.; Sun, Y. F. *Appl. Opt.* **2013**, *52*, 3937–3945.
- (24) Zhong, N. B.; Liao, Q.; Zhu, X.; Wang, Y. Z.; Chen, R. *Appl. Opt.* **2013**, *52*, 1432–1440.
- (25) Zhong, N. B.; Liao, Q.; Zhu, X.; Wang, Y. Z.; Chen, R. *Opt. Precis. Eng.* **2012**, *20*, 988–995 (Chinese)..
- (26) Bakke, R.; Olsson, P. Q. *J. Microbiol. Methods* **1986**, *5*, 93–98.
- (27) Chen, Y. H.; Huang, L.; Gan, L.; Li, Z. Y. *Light: Sci. Appl.* **2012**, *1*, e26.
- (28) Shin, S. J.; Lee, J. K.; Ha, H. Y.; Hong, S. A.; Chun, H. S. *J. Power Sources* **2002**, *106*, 146–152.
- (29) Polynkin, P.; Polynkin, A.; Peyghambarian, N.; Mansuripur, M. *Opt. Lett.* **2005**, *30*, 1273–1275.
- (30) Stoodley, P.; Sauer, K.; Davies, D. G.; Costerton, J. W. *Annu. Rev. Microbiol.* **2002**, *53*, 187–209.
- (31) Goeres, D. M.; Loetterle, L. R.; Hamilton, M. A.; Murga, R.; Kirby, D. W.; Donlan, R. M. *Microbiology* **2005**, *151* (3), 757–762.
- (32) Baniasadi, E.; Dincer, I.; Naterer, G. F. *Chem. Eng. J.* **2012**, *213*, 330–337.
- (33) Srinivasan, R.; Sailasuta, N.; Hurd, R.; Nelson, S.; Pelletier, D. *Brain* **2005**, *128*, 1016–1025.
- (34) Kim, T. J.; Young, B. M.; Young, G. M. *Appl. Environ. Microbiol.* **2008**, *74*, 5466–5474.
- (35) Lee, H. S.; Vermaas, W. F. J.; Rittmann, B. E. *Trends Biotechnol.* **2010**, *28*, 262–271.
- (36) Gavala, H. N.; Skiadas, I. V.; Ahring, B. K. *Int. J. Hydrogen Energy* **2006**, *31*, 1164–1175.